

SPECIAL PROJECT PROGRESS REPORT

Progress Reports should be 2 to 10 pages in length, depending on importance of the project. All the following mandatory information needs to be provided.

Reporting year 2018.....

Project Title: FLEXPART transport simulations and inverse modelling of atmospheric components.....
.....

Computer Project Account: SPNOFLEX.....

Principal Investigator(s): Espen Sollum.....
.....

Affiliation: NILU- Norwegian Institute for Air research.....

Name of ECMWF scientist(s) collaborating to the project (if applicable) Sabine Eckhardt, Massimo Cassiani, Rona Thompson, Ignacio Pisco, Arve Kylling, Andreas Stohl, Christine Groot Zwaafink, Nikolaos Evangeliou

Start date of the project: 2018.....

Expected end date: 2020.....

Computer resources allocated/used for the current year and the previous one (if applicable)

Please answer for all project resources

		Previous year		Current year	
		Allocated	Used	Allocated	Used
High Performance Computing Facility	(units)	100000		100000	
Data storage capacity	(Gbytes)	150		150	

Summary of project objectives

(10 lines max)

The Lagrangian particle dispersion model FLEXPART is run on ECMWF data to explore the transport and dispersion of various atmospheric constituents from greenhouse gases, radionuclides and aerosols like black carbon to volcanic ash released during eruptions. The model is used with various inversion techniques to infer emission estimates of many atmospheric compounds. This helps improving transport simulations of these substances and to understand their contribution and effects on the climate system.

Summary of problems encountered (if any)

(20 lines max)

.....

.....

.....

.....

.....

.....

Summary of results of the current year (from July of previous year to June of current year)

This section should comprise 1 to 8 pages and can be replaced by a short summary plus an existing scientific report on the project

1) Implementation, Test and Case study of a wet deposition algorithm in backward mode.

Existing Lagrangian particle dispersion models are capable of establishing source-receptor relationships by running either forward or backward in time. For receptor-oriented studies such as interpretation of “point” measurement data, backward simulations can be computationally more efficient by several orders of magnitude. However, to date, the backward modelling capabilities have been limited to atmospheric concentrations or mixing ratios. We extend the backward modelling technique to substances deposited at the Earth’s surface by wet scavenging and dry deposition. This facilitates efficient calculation of emission sensitivities for deposition quantities at individual sites, which opens new application fields such as the comprehensive analysis of measured deposition quantities, or of deposition recorded in snow samples or ice cores. This could also include inverse modelling of emission sources based on such measurements. We have tested the new scheme as implemented in the Lagrangian particle dispersion model FLEXPART v10.2 by comparing results from forward and backward calculations.

For this study, we used three-hourly ERA-Interim re-analysis data from ECMWF with a resolution of 1° latitude x 1° longitude and 61 vertical levels. Figure 1 shows the emission flux of the inventory used (Fig. 1a), the average concentration in the lowest model layer (0-100 m above ground level) (Fig. 1b), and the accumulated wet (Fig. 4c) and dry deposition (Fig. 1d) for March 2012. Based on these results, we selected two locations where we compare the results for forward and backward simulations. The two points represent very different concentration and deposition levels, due to their different distances from strong BC source regions. While point A is located relatively close to strong emission sources (average concentration of 270 ng m^{-3}), point B on Spitsbergen in the Arctic is far away from sources (average concentration of 7 ng m^{-3}).

In general, the forward and backward simulations show very good agreement for both receptor points. For example, the distinct daily cycles in concentration and dry deposition at point A are simulated similarly, and the mean concentration and deposition values are almost identical in the forward and backward simulations at both points. However, during some episodes there can be notable differences, for example at the end of the simulation period at point A.

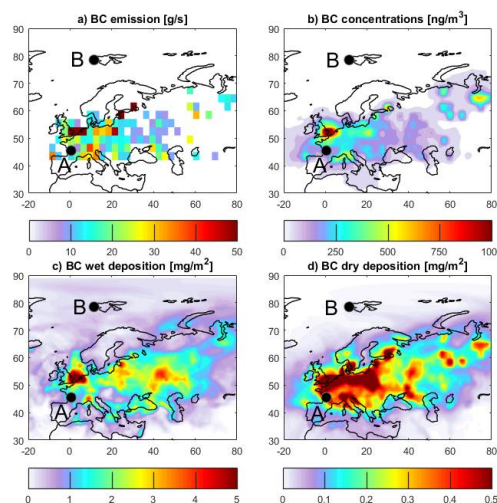


Figure 1: Average BC emission fluxes (a), average BC concentrations in the lowest model layer (0-100 m) (b), accumulated BC wet deposition (c) and accumulated BC dry deposition (d) for the period of 1 March to 1 April 2012. The black dots show the locations A and B for which a detailed comparison of forward and backward calculations is performed.

2) Transport of Black Carbon (BC) in the Greenland Ice Sheet from the 2017 fires in Greenland

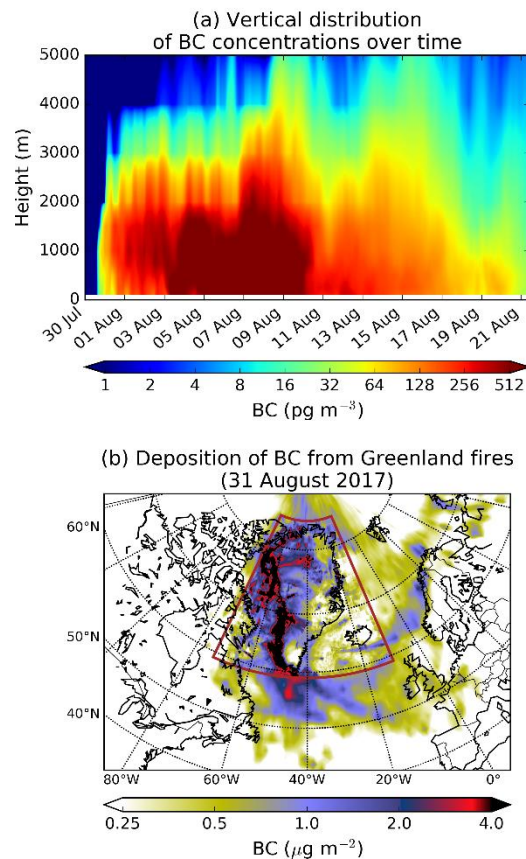


Figure 2. (a) Time-series of vertical distribution of BC concentrations averaged over the area of Greenland in summer 2017 as a function of time. (b) Total (wet and dry) deposition of BC (in $\mu\text{g m}^{-2}$) from Greenland fires until 31 August 2017. The colored rectangle depicts the nested high-resolution domain.

We simulated highly-unusual open fires that burned in Western Greenland between 31 July and 21 August 2017, after a period of warm, dry and sunny weather. The fires burned on peat lands that became vulnerable to fires by permafrost thawing. We used several satellite data sets to estimate that the total area burned was about 2345 hectares. Based on assumptions of typical burn depths and BC emission factors for peat fires, we estimate that the fires consumed a fuel amount of about 117 kt C and produced BC emissions of about 23.5 t. We used the Lagrangian particle dispersion model FLEXPART to simulate the atmospheric BC transport and deposition (Figure 2) driven by hourly $0.5^\circ \times 0.5^\circ$ operational analyses from the European Centre for Medium-Range Weather Forecasts (ECMWF). Concentration and deposition fields were recorded in a global domain of $1^\circ \times 1^\circ$ spatial resolution with three hourly outputs. To capture the spatiotemporal variability of BC over the Greenland Ice Sheet, a nested domain with $0.05^\circ \times 0.05^\circ$ resolution was used.

We find that the smoke plumes were often pushed towards the Greenland Ice Sheet by westerly winds and thus a large fraction of the BC emissions (7 t or 30%) was deposited on snow or ice covered surfaces. The calculated BC deposition was small compared to BC deposition from global sources, but not entirely negligible.

3) Inverse modeling of Black Carbon (BC) in high northern latitudes in 2013–2015 time period

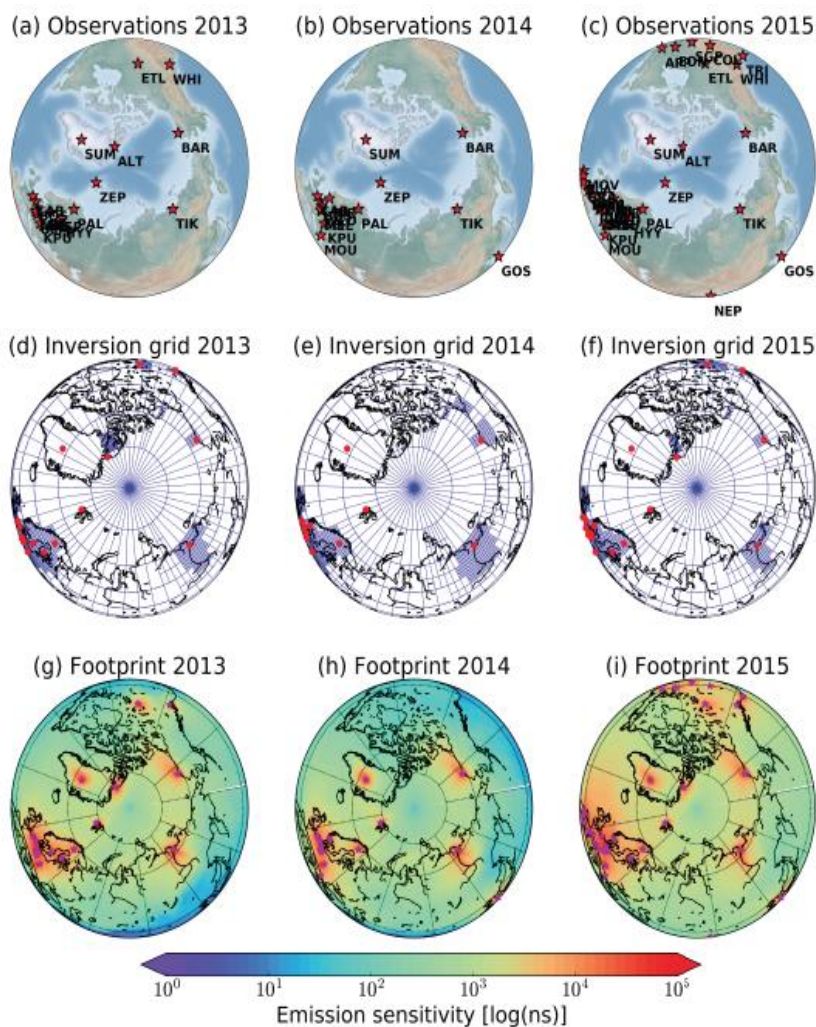


Figure 3. Observation network used for the present inversion (a, b and c), and variable-resolution grid used for the inversion (d, e, and f) also showing the location of the observation sites (red stars) for 2013–2015 period. Sensitivity to the surface emissions (i.e., the footprint emission sensitivity or equivalently source-receptor relationship) integrated over all observation sites and all time steps (g, h and i) for

We conducted BC inversions at high northern latitudes ($>50^\circ\text{N}$) for the 2013–2015 period. A sensitivity analysis was performed to select the best representative species for BC and the best prior emission dataset. The same model ensemble was used to assess the uncertainty of the posterior emissions of BC due to scavenging and removal and due to the use of different prior emission inventory. The source-receptor relationships for the Bayesian inversion were calculated using the Lagrangian particle dispersion model FLEXPART (Figure) driven with European Centre for Medium-Range Weather Forecasts operational meteorological analyses from the Integrated Forecast System (IFS) with 137 model levels and a horizontal resolution of $0.5^\circ \times 0.5^\circ$. The optimised emissions of BC were high close to the gas flaring regions in Russia and in Western Canada (Alberta), where numerous power and oil/gas production industries operate. The annual posterior emissions of BC at latitudes above 50°N were estimated as 560 ± 171 kt yr $^{-1}$, significantly smaller than in ECLIPSEv5 (745 kt yr $^{-1}$), which was used and the prior information in the inversions of BC. The average relative uncertainty of the inversions was estimated to be 30%.

Posterior concentrations of BC simulated over Arctic regions were compared with independent observations from flight and ship campaigns showing, in all cases, smaller bias, which in turn witnesses the success of the inversion. Posterior emissions of BC in North America are driven by anthropogenic sources, while biomass burning appeared to be less significant as it is also confirmed by satellite products. In North Europe, posterior emissions were estimated to be half compared to the prior ones, with the highest releases to be in megacities and due to biomass burning in Eastern Europe. The largest emissions of BC in Siberia were calculated along the transect between Yekaterinsburg and Chelyabinsk. Flaring emissions in Nenets-Komi oblast (Russia) were estimated to be much lower than in the prior emissions, while in Khanty-Mansiysk (Russia) they remained the same after the inversions of BC. Increased emissions in the borders between Russia and Mongolia are probably due to biomass burning in villages along the Trans-Siberian Railway.

4) Radiative forcing by mineral dust

Mineral dust sources at high and low latitudes contribute to atmospheric dust loads and dust deposition in the Arctic. With dust load estimates from Groot Zwaafink et al. (2016), we quantify the mineral dust instantaneous radiative forcing (IRF) in the Arctic for the year 2012. The full study was presented by Kylling et al. (2018). Meteorological input data for simulations with the dust emission model FLEXDUST, the atmospheric transport model FLEXPART and the radiative transfer model libRadtran were ECMWF operational analysis fields at 1 degree resolution. Results show that the annual-mean top of the atmosphere IRF is 0.225 W m^{-2} , with the largest contributions from dust transported from Asia south of 60°N and Africa (see Fig. 4). High-latitude ($>60^\circ\text{N}$) dust sources contribute about 39% to top of the atmosphere IRF and have a larger impact (1 to 2 orders of magnitude) on IRF per emitted kilogram of dust than low-latitude sources. Mineral dust deposited on snow accounts for nearly all of the bottom of the atmosphere IRF of 0.135 W m^{-2} . More than half of the bottom of the atmosphere IRF is caused by dust from high-latitude sources, indicating substantial regional climate impacts rarely accounted for in current climate models.

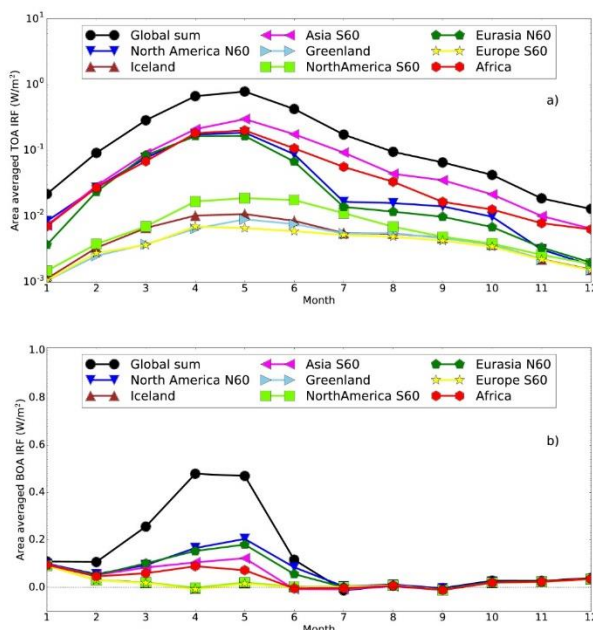


Figure 4: Individual contributions from various regions to the top of the atmosphere (TOA) (a) and bottom of the atmosphere (BOA) (b) dust instantaneous radiative forcing (IRF) for the year 2012. Note the logarithmic scale on y axis in panel (a). The black dotted line in panel (b) indicates the zero line. Figure 3 from Kylling et al. (2018).

List of publications/reports from the project with complete references

Eckhardt, S., M. Cassiani, N. Evangeliou, E. Sollum, I. Pisso, and A. Stohl (2017): Source-receptor matrix calculation for deposited mass with the Lagrangian particle dispersion model FLEXPART v10.2 in backward mode. *Geophys. Mod. Dev.* 10, 4605–4618, doi:10.5194/gmd-10-4605-2017

Evangeliou, N., Kylling, A., Eckhardt, S., Myrioniuk, V., Stebel, K., Paugam, R., Zibtev, S., and Stohl, A.: Open fires in Greenland: an unusual event and its impact on the albedo of the Greenland Ice Sheet, *Atmos. Chem. Phys. Discuss.*, <https://doi.org/10.5194/acp-2018-94>, in review, 2018.

Evangeliou, N., Thompson, R. L., Eckhardt, S., and Stohl, A.: Top-down estimates of black carbon emissions at high latitudes using an atmospheric transport model and a Bayesian inversion framework, *Atmos. Chem. Phys. Discuss.* submitted, 2018.

Groot Zwaafink, C. D., H. Grythe, H. Skov, A. Stohl, (2016) Substantial contribution of northern high-latitude sources to mineral dust in the Arctic, *Journal of Geophysical Research*, 121, 13,678–13,697, DOI: 10.1002/2016JD025482

Kylling A., C.D. GrootZwaafink, and A. Stohl (2018), 'Mineral dust instantaneous radiative forcing in the Arctic', *Geophys. Res. Lett.*, 45, doi:10.1029/2018GL077346.

Summary of plans for the continuation of the project

(10 lines max)

The newly implemented algorithm for deposition calculation in backward mode will be applied to analyse deposition measurements in the Arctic (e.g. ice cores). CO_2 inversion, facilitation the FLEXPART model and the FLEXINVERT tools will be performed.